

Radius of curvature uncertainty: Nonlinear measurand and treatment

Tony L. Schmitz^a and Angela Davies^b

^aDepartment of Mechanical and Aerospace Engineering, University of Florida, Gainesville, FL 32611

^bDepartment of Physics and Optical Science, University of North Carolina at Charlotte, Charlotte, NC 28223

1.0 Introduction

The radius of curvature of an optical element is one of the dominant parameters that determines optical power and must be well-characterized if accurate results are to be obtained from ray trace models of complex systems. Radius errors can be partially compensated by element respacing during assembly, but this is time-consuming and costly and can lead to unwanted wavefront aberrations. For spherical components, radius is usually defined by the least-squares best-fit radius of the sphere over the clear aperture. Many measurement methods are available, including comparison with ‘known radius’ test plates, direct image formation/knife-edge test, astigmatism measurement, spherometers, autocollimator with pentaprism, and shearing interferometers, but the optical radius bench generally gives the lowest uncertainty [1-2].

Optical bench measurements are carried out using a figure measuring interferometer to identify two critical positions of the test artifact, confocal and cat’s eye. The reflected wavefront matches the wavefront exiting the interferometer at these two locations, resulting in a nulled cavity. A linear transducer, often a displacement measuring interferometer or DMI, measures the displacement of the stage/part between the two positions and the recorded distance nominally represents the radius of the best-fit sphere to the surface. This measurement is shown schematically in Fig. 1 (after [3]), where the confocal and cat’s eye positions are identified by a linear regression to the (circular aperture) Zernike polynomial a_2^0 , or power, terms recorded at a discrete number of locations along the optical, or z , axis of the interferometer (the corresponding DMI values are also recorded).

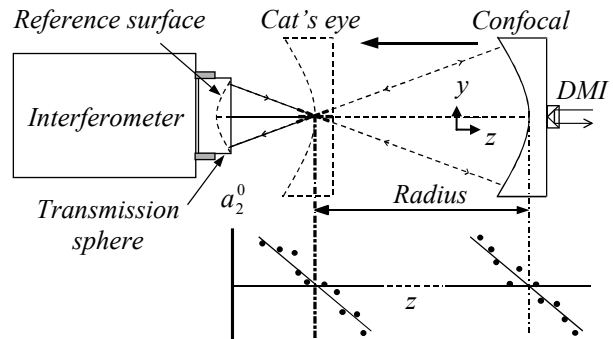


Figure 1: Schematic of optical bench measurement using a Fizeau interferometer.

To carry out a traceable radius measurement, however, all biases must be corrected and uncertainty sources combined to yield the combined standard uncertainty, u_c , which represents one standard deviation of the measurand, or quantity under test [3-7]. In an effort to properly define the measurand for optical bench measurements, we have implemented a homogeneous transformation matrix (HTM) formalism, where a vector equation is used to define the radius and an HTM is used to determine the location of the test artifact after translation from confocal to cat’s eye. It is shown that for the nonlinear measurand equation generated by this approach, it is not possible to simply insert expectation values for each uncertainty contributor to determine the best estimate of the measurement variance. Rather, a Monte Carlo simulation is applied to determine the expected measurement variance.

To carry out a traceable radius measurement, however, all biases must be corrected and uncertainty sources combined to yield the combined standard uncertainty, u_c , which represents one standard deviation of the measurand, or quantity under test [3-7]. In an effort to properly define the measurand for optical bench measurements, we have implemented a homogeneous transformation matrix (HTM) formalism, where a vector equation is used to define the radius and an HTM is used to determine the location of the test artifact after translation from confocal to cat’s eye. It is shown that for the nonlinear measurand equation generated by this approach, it is not possible to simply insert expectation values for each uncertainty contributor to determine the best estimate of the measurement variance. Rather, a Monte Carlo simulation is applied to determine the expected measurement variance.

2.0 Radius equation description

There are many potential sources of radius uncertainty and measurement bias, such as wavefront aberrations, null identification at confocal and cat’s eye, artifact figure error, displacement gage error, and stage error motions [3, 6-7]. Error motions are particularly challenging because they are interrelated and convolved with the measurement. Recent work has focused on identifying uncertainty contributions, removing measurement biases, and determining the uncertainty through a root-sum-of-the-squares (RSS) combination [3, 7]. However, an equation that explicitly defines radius as a function of all uncertainty sources was not implemented. In the HTM approach presented here, the measurand, R , is represented by a vector equation that intrinsically corrects for error motions and allows other uncertainty contributors to be conveniently represented.

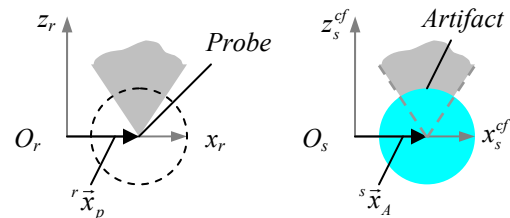


Figure 2: Coordinate frame identification for the confocal position. Reference and stage frames overlap at this location.

In the HTM approach presented here, the measurand, R , is represented by a vector equation that intrinsically corrects for error motions and allows other uncertainty contributors to be conveniently represented.

Formulation of the HTM-based radius equation begins with identification of the necessary coordinates and frames (similar to kinematic error analyses for precision machine tools, robots, and stages [8]). These include the reference, r , and stage, s , frames and their origins, O_r and O_s , respectively, and the probe, p , and artifact, A , coordinates, where p is assumed to be located at the geometric focus of the interferometer and A at the artifact best-fit center. Figure 2 shows the frames and origins for the confocal position, as well as the vectors ${}^r\vec{x}_p$ and ${}^s\vec{x}_A$, which locate the probe in the reference frame and artifact center in the stage frame, respectively. Two measurement scenarios are depicted in Fig. 3.

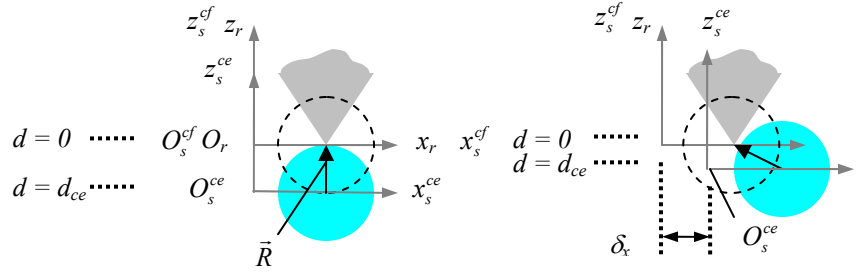


Figure 3: (Left) error free radius measurement; (right) straightness error introduces measurement bias.

For the left figure, there is perfect translation between confocal and cat's eye along the z_r axis. In this case, the displacement gage reading at cat's eye, d_{ce} , is equal to the radius amplitude, R . In the right figure, an x -direction straightness error, δ_x , is imposed and the gage reading is now less than the true radius (i.e., a measurement bias is introduced).

The straightness error scenario is reproduced in Fig. 4 to describe the vector radius equation. The figure shows that the radius can be expressed as the vector difference, $\vec{R} = {}^r\vec{x}_p - {}^r\vec{x}_A$, and the amplitude by $R = |\vec{R}| = \sqrt{|{}^r\vec{x}_p - {}^r\vec{x}_A|^2}$. To solve these equations, it is necessary to express ${}^r\vec{x}_p$ and ${}^r\vec{x}_A$ in terms of measurable quantities. We can express the latter using an HTM, populated by separate measurements of the stage error motions, to map the artifact center's location at cat's eye to the reference coordinate system. The required HTM is the following:

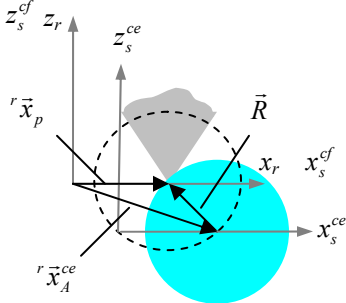


Figure 4: Vector radius description.

$${}^rT_s = \begin{bmatrix} 1 & -\varepsilon_z & \varepsilon_y & \delta_x \\ \varepsilon_z & 1 & -\varepsilon_x & \delta_y \\ -\varepsilon_y & \varepsilon_x & 1 & \delta_z + d \\ 0 & 0 & 0 & 1 \end{bmatrix}, \quad (1)$$

where the ε_j terms represent small, rigid body rotations about the j^{th} axis during z -direction motion of the stage (relative to the reference frame) and the δ_j terms represent 1) small, rigid body displacements in the j^{th} axis during z -direction motion of the stage (relative to the reference frame) and/or 2) misalignment between the gage axis and reference frame (i.e., traditional cosine error). We can then write ${}^r\vec{x}_A = {}^rT_s {}^s\vec{x}_A$. In this equation, the artifact center in the stage frame, ${}^s\vec{x}_A$, may be written as a function of probe offsets in the reference frame and the ability to null at the confocal position, dx^{cf} , dy^{cf} , and dz^{cf} (note that the reference and stage frames ideally overlap at confocal). After these substitutions, the final vector equation can be written as shown in Eq. 2, where R^2 is determined from the sum-of-the-squares of the x , y , and z -direction components of the right hand side.

$$\vec{R} = {}^r\vec{x}_p - {}^rT_s \begin{pmatrix} {}^r\vec{x}_p + \begin{bmatrix} dx^{cf} \\ dy^{cf} \\ dz^{cf} \\ 1 \end{bmatrix} \end{pmatrix} = \begin{bmatrix} -dx^{cf} + \varepsilon_z({}^r y_p + dy^{cf}) - \varepsilon_y({}^r z_p + dz^{cf}) - \delta_x + 0 \\ -dy^{cf} - \varepsilon_z({}^r x_p + dx^{cf}) + \varepsilon_x({}^r z_p + dz^{cf}) - \delta_y + 0 \\ -dz^{cf} + \varepsilon_y({}^r x_p + dx^{cf}) - \varepsilon_x({}^r y_p + dy^{cf}) - \delta_z - d \\ 1 \end{bmatrix} \quad (2)$$

2.1 Analytical expectation value

Four error categories are identified in Eq. 2. The translational errors in column I represent the ability to null at confocal. Category II groups the Abbe errors (rotation-offset products), while category III gives the straightness/cosine errors. The fourth column consists of the gage reading for z -direction motions. Equation 2 is expanded in Eq. 3 to give the final R expression. To simplify this expression, we have set the terms containing δ_z , which represents positioning error along the reference axis, and ${}^r z_p$, the probe offset in the z -direction expressed in the reference frame, equal to zero. The positioning error along the z -axis is accounted for by calibrating the displacement gauge with some uncertainty. We assume the error motions depend only linearly on the z -position. Therefore, the location of $z = 0$ is arbitrary and ${}^r z_p$ can be set to zero.

$$R = \left(\begin{aligned} & d_{ce}^2 + \delta_x^2 + \delta_y^2 + dx^{cf^2} + dy^{cf^2} + dz^{cf^2} + 2dx^{cf}\delta_x + 2dy^{cf}\delta_y + 2dz^{cf}d_{ce} + \\ & \varepsilon_z^2 \left({}^r y_p^2 + 2{}^r y_p dy^{cf} + dy^{cf^2} \right) + \varepsilon_z^2 \left({}^r x_p^2 + 2{}^r x_p dx^{cf} + dx^{cf^2} \right) + \\ & \varepsilon_y^2 \left({}^r x_p^2 + 2{}^r x_p dx^{cf} + dx^{cf^2} \right) + \varepsilon_x^2 \left({}^r y_p^2 + 2{}^r y_p dy^{cf} + dy^{cf^2} \right) + \varepsilon_x^2 \left(dz^{cf^2} \right) + \varepsilon_y^2 \left(dz^{cf^2} \right) + \\ & 2\varepsilon_z \delta_y {}^r x_p - 2\varepsilon_z \delta_x {}^r y_p + 2\varepsilon_x {}^r y_p d_{ce} - 2\varepsilon_y {}^r x_p d_{ce} + 2dy^{cf}\varepsilon_x d_{ce} - 2dx^{cf}\varepsilon_y d_{ce} + \\ & 2dy^{cf}\varepsilon_z \left({}^r x_p - \delta_x \right) - 2dx^{cf}\varepsilon_z \left({}^r y_p - \delta_y \right) + 2dz^{cf}\varepsilon_x \left({}^r y_p - \delta_y \right) - 2dz^{cf}\varepsilon_y \left({}^r x_p - \delta_x \right) - \\ & \left(2\varepsilon_x \varepsilon_y \left({}^r x_p {}^r y_p + {}^r x_p dy^{cf} + {}^r y_p dx^{cf} + dx^{cf} dy^{cf} \right) - 2\varepsilon_x \varepsilon_z \left({}^r x_p dz^{cf} + dx^{cf} dz^{cf} \right) - 2\varepsilon_y \varepsilon_z \left({}^r y_p dz^{cf} + dy^{cf} dz^{cf} \right) \right) \end{aligned} \right)^{\frac{1}{2}} \quad (3)$$

Given this expression for R , a logical next step would be to determine the best estimate of a measured radius by evaluating the equation for each term on the right hand side by using the expectation value, which is defined as the product of the parameter and its probability distribution integrated over all possible values [9]. Although it may not be the case in general, for the discussion here we will assume here that all errors are zero on average and the gage axis is collinear with the motion axis (recall that a misalignment will introduce a linear term into the straightness values). The expectation value of each non-squared errors is, therefore, zero. By applying this assumption and neglecting terms that are products of higher order (these terms would be small for a well-designed system), Eq. 3 can be approximated as shown in Eq. 4. The reader may note that the squared terms remain because the expectation values are not zero, but rather are equal to the variance (or square of the standard deviation).

$$R \approx \left(\begin{aligned} & d_{ce}^2 + \delta_x^2 + \delta_y^2 + dx^{cf^2} + dy^{cf^2} + dz^{cf^2} + \\ & \varepsilon_z^2 \left({}^r y_p^2 + dy^{cf^2} \right) + \varepsilon_z^2 \left({}^r x_p^2 + dx^{cf^2} \right) + \\ & \varepsilon_y^2 \left({}^r x_p^2 + dx^{cf^2} \right) + \varepsilon_x^2 \left({}^r y_p^2 + dy^{cf^2} \right) + \varepsilon_x^2 \left(dz^{cf^2} \right) + \varepsilon_y^2 \left(dz^{cf^2} \right) \end{aligned} \right)^{\frac{1}{2}} \quad (4)$$

To determine the expectation value for R , common practice would be to substitute the expectation value for each input on the right hand side of Eq. 4. In fact, some of the remaining terms make this an appealing option. For example, the presence of the straightness error, δ_x , would account for the bias shown in Fig. 3 which causes the gage reading to be less than the actual radius amplitude. The reported measurement value, R , is compensated for this error since it is summed in quadrature with d_{ce} (which would otherwise be used as the reported radius value). *However, due to the nonlinear nature of the radius equation, this direct term-by-term expectation value substitution cannot be applied.* The error is revealed if we consider the dz^{cf^2} term. Recall that dz^{cf} is the ability to null the confocal position at the beginning of the optical bench measurements. Let's assume that all other error contributions are exactly zero. If this z -direction error is taken to have a mean zero and normal distribution with standard deviation σ_{dz} , we would expect the measured radius to be equal to the mean gage reading (recorded along the z axis) with a normal distribution and standard deviation σ_{dz} . However, Eq. 4 suggests that a bias in R dependent on σ_{dz}^2 would be introduced. This is clearly not the case and highlights the invalidity of this approach. Said another way, for a generic

parameter x , to which is added noise δx with a mean of 0, the best estimate for x is $x = \sqrt{\langle (x + \delta x)^2 \rangle}$ which is *not* equal to $\sqrt{\langle (x + \delta x)^2 \rangle}$ (where the angled brackets represent the expectation value).

2.2 Monte Carlo analysis

For situations like this where the measurand equation is complicated and nonlinear, we recommend a Monte Carlo simulation to directly evaluate the mean and standard deviation in R given the input distributions and mean values of the inputs to Eq. 3 (no truncation of the original equation need be applied). Estimates of the expected values, uncertainties, and the form of the probability distribution (usually Gaussian) for each term in Eq. 3 are needed to carry out the simulation and estimate R for a particular measurement. A Monte Carlo analysis shows that the category I and III terms in Eq. 2 give single-sided (biased) distributions in R for the x and y -direction components, but unbiased results for the z terms. See Figs. 5 and 6, where 100,000 points and zero probe offsets were applied in the simulations. These results agree with the intuitive description provided in Section 2.1 and verify that a direct analytic substitution into the nonlinear Eq. 3 yields incorrect results.

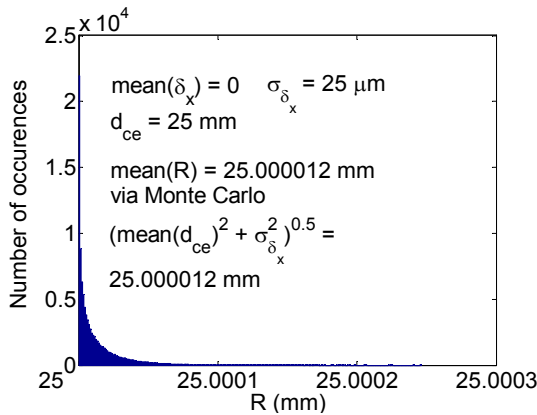


Figure 5: Histogram of Monte Carlo results for mean zero δ_x error with standard deviation of $25 \mu\text{m}$. A single-sided (biased) distribution is observed.

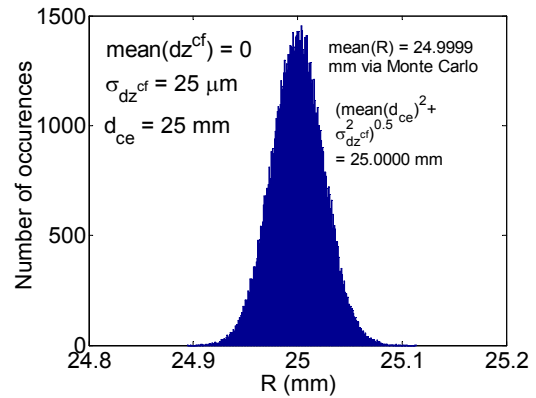


Figure 6: Histogram for dz^{cf} error with zero mean and $25 \mu\text{m}$ standard deviation. No bias is introduced in this case.

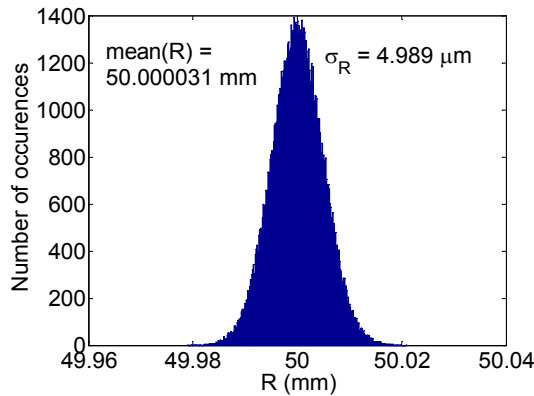


Figure 7: Monte Carlo simulation results for measurement described in Table 1.

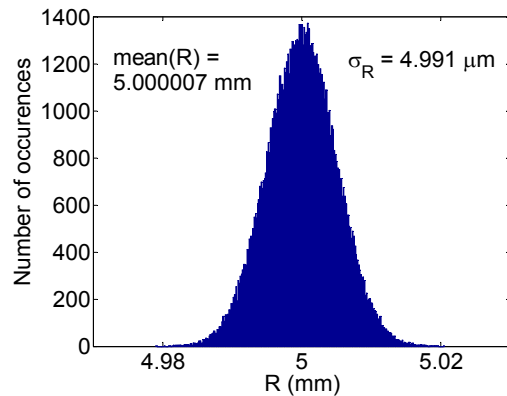


Figure 8: Monte Carlo results for $d_{ce} = 5 \text{ mm}$.

2.3 Uncertainty evaluation

Two options may be considered to determine $u_c(R)$ from Eq. 3. Following the ISO GUM [4] recommendations, the Taylor series expansion of R can be completed and the standard uncertainties in each variable inserted into the

result and multiplied by the corresponding sensitivity coefficient (i.e., the partial derivative of R with respect to the input variable in question). This would be extremely difficult. Instead, the distribution of R values that results from the Monte Carlo simulation directly reflects the combined standard uncertainty. In other words, by defining the mean, standard deviation, and distribution of each input to Eq. 3 using Type A (statistical) or Type B (other) approaches [4-5], the resulting standard deviation from the Monte Carlo simulation is u_c . As an example, the distribution of R values shown in Fig. 7 is the simulation result for the normally distributed inputs shown in Table 1. Although x and y -direction straightness and confocal null errors are present, this distribution is not single-sided. This is due to the nonzero z error standard deviations. The standard deviation of the 100,000 Monte Carlo simulation data points is $5.0 \mu\text{m}$; therefore, $u_c(R) = 5.0 \mu\text{m}$ (0.01% of the mean) for the conditions given in Table 1. As a comparison, this was repeated for $d_{ce} = 5 \text{ mm}$ using the same input uncertainties (this is reasonable since the uncertainties are based on our ability to measure the individual uncertainty contributors and not always directly on the size of the artifact in question) – see Fig. 8. In this case, the mean R was 5.000007 mm and $u_c(R)$ was $5.0 \mu\text{m}$ (0.1%). This underscores the importance of improved optical bench characterization and/or precision construction for measurement of small radii.

Table 1: Input values for Monte Carlo simulation.

Input	Mean	Standard deviation
${}^r x_p$	2 mm	$50 \mu\text{m}$
${}^r y_p$	2 mm	$50 \mu\text{m}$
${}^r z_p$	0	$50 \mu\text{m}$
d_{ce}	50 mm	50 nm
dx^{cf}	0	$1 \mu\text{m}$
dy^{cf}	0	$1 \mu\text{m}$
dz^{cf}	0	$5 \mu\text{m}$
δ_x	0	$1 \mu\text{m}$
δ_y	0	$1 \mu\text{m}$
δ_z	0	0
ε_x	0	$5 \mu\text{rad}$
ε_y	0	$5 \mu\text{rad}$
ε_z	0	$5 \mu\text{rad}$

3.0 Conclusions

In this paper, we described an HTM-based vector equation which defines the measurand in optical bench radius measurements for spherical optics. It was shown that for the corresponding nonlinear radius equation, direct substitution in order to analytically determine the expectation value leads to erroneous results. Additionally, the use of Taylor series expansion of the measurand to determine the combined standard uncertainty is not recommended. As an alternative, Monte Carlo simulations are successfully applied to conveniently find both the mean and standard deviation, which represents the combined standard uncertainty, of the radius. This was illustrated for multiple cases.

4.0 Acknowledgements

The authors wish to acknowledge helpful discussions with W. T. Ester, National Institute of Standards and Technology, Gaithersburg, MD, and C. J. Evans, Zygo

Corporation, Middlefield, CT, during this work.

5.0 References

1. Malacara, D., 1992, *Optical Shop Testing*, John Wiley & Sons, New York.
2. Murty, M. and Shukla, R., 1983, Measurements of long radius of curvature, *Optical Engineering*, **22**: 231-235.
3. Schmitz, T. L., Evans, C. J., Davies, A., and Estler, W. T., 2002, Displacement uncertainty in interferometric radius measurements, *Annals of the CIRP*, **51**/1: 451-454.
4. International Organization for Standardization (ISO), 1995, *Guide to the Expression of Uncertainty in Measurement*, Geneva.
5. Taylor, B. and Kuyatt, C., 1994, NIST Technical Note 1297, *Guidelines for Evaluating and Expressing the Uncertainty of NIST Measurement Results*.
6. Selberg, L., 1992, Radius measurement by interferometry, *Optical Engineering*, **31**: 1961-1966.
7. Schmitz, T. L., Davies, A., and Evans, C. J., 2001, Uncertainties in interferometric measurements of radius of curvature, *Optical Manufacturing and Testing IV*, Stahl, H. P., Editor, *Proceedings of SPIE*, **4451**: 432-447.
8. Slocum, A., 1992, *Precision Machine Design*, Prentice-Hall, Englewood Cliffs, NJ.
9. Bevington, P. R. and Robinson, D. K., 1992, *Data Reduction and Error Analysis for the Physical Sciences*, 2nd Ed., WCB/McGraw-Hill, New York.